Purinergic Signalling (2023) 19:565–578
https://doi.org/10.1007/s11302-022-09873-3

ORIGINAL ARTICLE

Fluorescent A_{2A} and A_3 adenosine receptor antagonists as flow cytometry probes

Kiran S. Toti[1,2] · Ryan G. Campbell[1] · Hobin Lee[1] · Veronica Salmaso[1] · R. Rama Suresh[1] · Zhan-Guo Gao[1] · Kenneth A. Jacobson[1]

Received: 25 March 2022 / Accepted: 24 May 2022 / Published online: 10 June 2022

Abstract

Adenosine receptor (AR) ligands are being developed for metabolic, cardiovascular, neurological, and inflammatory diseases and cancer. The ease of drug discovery is contingent on the availability of pharmacological tools. Fluorescent antagonist ligands for the human A_{2A} and A_3ARs were synthesized using two validated pharmacophores, 1,3-dipropyl-8-phenylxanthine and triazolo[1,5-c]quinazolin-5-yl)amine, which were coupled to eight reporter fluorophores: AlexaFluor, JaneliaFluor (JF), cyanine, and near infrared (NIR) dyes. The conjugates were first screened using radioligand binding in HEK293 cells expressing one of the three AR subtypes. The highest affinities at A_{2A}AR were K_i 144–316 nM for **10**, **12**, and **19**, and at A_3AR affinity of K_i 21.6 nM for **19**. Specific binding of JF646 conjugate MRS7774 **12** to the HEK293 cell surface A_{2A}AR was imaged using confocal microscopy. Compound **19** MRS7535, a triazolo[1,5-c]quinazolin-5-yl)amine containing a Sulfo-Cy7 NIR dye, was suitable for A_3AR characterization in whole cells by flow cytometry (K_d 11.8 nM), and its bitopic interaction mode with an A_3AR homology model was predicted. Given its affinity and selectivity (11-fold vs. A_{2A}AR, ~ 50-fold vs. A_1AR and A_{2B}AR) and a good specific-to-nonspecific binding ratio, **19** could be useful for live cell or potentially a diagnostic in vivo NIR imaging tool and/or therapy targeting the A_3AR.

Keywords Adenosine receptor · Antagonist · Receptor binding · Fluorescent ligands · Drug discovery · Flow cytometry

Kiran S. Toti, was a post-doctoral fellow in Dr Jacobson's research group at NIH, USA, from 2014-2020. He holds a PhD degree from Ghent University, Belgium, for the dissertation titled 'Synthesis and Biological Evaluation of 4-Hydroxymethyl Deleted, Transposed and Modified Nucleosides' under the guidance of Prof. Serge Van Calenbergh. Kiran has 10+ years medicinal chemistry research experience working on GPCR, kinase and polymerase small molecule modulators involving nucleosi(t)ides and heterocycles. At present, he is an Assoc. Scientist in the group of Prof. Dennis Liotta at the Chemistry Department, Emory University.

✉ Kenneth A. Jacobson
kennethj@niddk.nih.gov

[1] Molecular Recognition Section, Laboratory of Bioorganic Chemistry, National Institute of Diabetes and Digestive and Kidney Diseases, National Institutes of Health, NIH, NIDDK, LBC, Bldg. 8A, Rm. B1A-19, Bethesda, MD 20892-0810, USA

[2] Current Address: Chemistry Department, Emory University, 1093 Rollins Research Center, Atlanta, GA 30322, USA

Abbreviations

AN	Acetonitrile
AR	Adenosine receptor
BY	BODIPY (4,4-difluoro-4-bora-3a,4a-diaza-s-indacene)
CGS15943	9-Chloro-2-(furan-2-yl)-[1,2,4]triazolo[1,5-*c*]quinazolin-5-amine
CGS21680	2-[*p*-(2-Carboxyethyl)phenylethylamino]-5′-*N*-ethylcarboxamido-adenosine
DIPEA	Diisopropylethylamine
DMEM	Dulbecco's modified Eagle medium
DMF	*N*,*N*-Dimethylformamide
DPCPX	Cyclopentyl-1,3-dipropylxanthine
EL	Extracellular loop
IE	Interaction energy
FBS	Fetal bovine serum
GPCR	G protein-coupled receptor
HEK	Human embryonic kidney
I-AB-MECA	N^6-(4-Amino-3-iodobenzyl) adenosine-5′-*N*-methyluronamide
MD	Molecular dynamics
MFI	Mean fluorescence intensity
NHS	*N*-Hydroxysuccinimide
NIR	Near infrared
RMSD	Root mean squared deviation
TEAA	Triethylammonium acetate
TFA	Trifluoroacetic acid
TFP	2,3,5,6-Tetrafluorophenyl
TM	Transmembrane helical domain
XAC	N-(2-aminoethyl)-2-[4-(2,6-dioxo-1,3-dipropyl-2,3,6,7-tetrahydro-1H-purin-8-yl) phenoxy]acetamide
ZM241385	4-[2-[7-Amino-2-(2-furyl)-1,2,4-triazolo[1,5-*a*][1,3,5]triazin-5-yl-amino] ethyl]phenol

Introduction

Fluorescent ligands of the adenosine receptor (AR) family have provided insights into the orthosteric and allosteric ligand binding sites and receptor dimerization that conventional radioligands could not achieve [1–3]. The first high affinity fluorescent ligand of an adenosine receptor **1** (Fig. 1) was for the A_{2A}AR, based on the ability of the terminal carboxylate group of selective agonist CGS21680 to be extended through amides without loss of binding affinity [4]. Other agonist fluorescent ligands in the same structural class, such as **2**, were used to detect A_{2A}AR heterodimerization with the D_2 dopamine receptor [5]. A fluorescent N^6-substituted A_3AR agonist, **3**, was used to characterize receptor-receptor interactions in A_3AR homodimers [6]. Antagonist fluorescent ligands have been reported for the A_1AR, A_{2A}AR, A_{2B}AR, and A_3AR [7–14]. These probes, such as triazolo[1,5-c]quinazolin-5-yl)amine MRS5449 **5**, facilitate drug screening using flow cytometry of whole cells and other techniques to discover novel antagonists [8]. The bitopic nature of these fluorescent-tethered ligands often causes deviation from the simple bimolecular interaction between ligand and target receptor, as was shown for various A_{2A}AR antagonists [13]. The binding of the fluorophore moiety can allosterically modulate the pharmacophore affinity at the orthosteric site, depending on precise

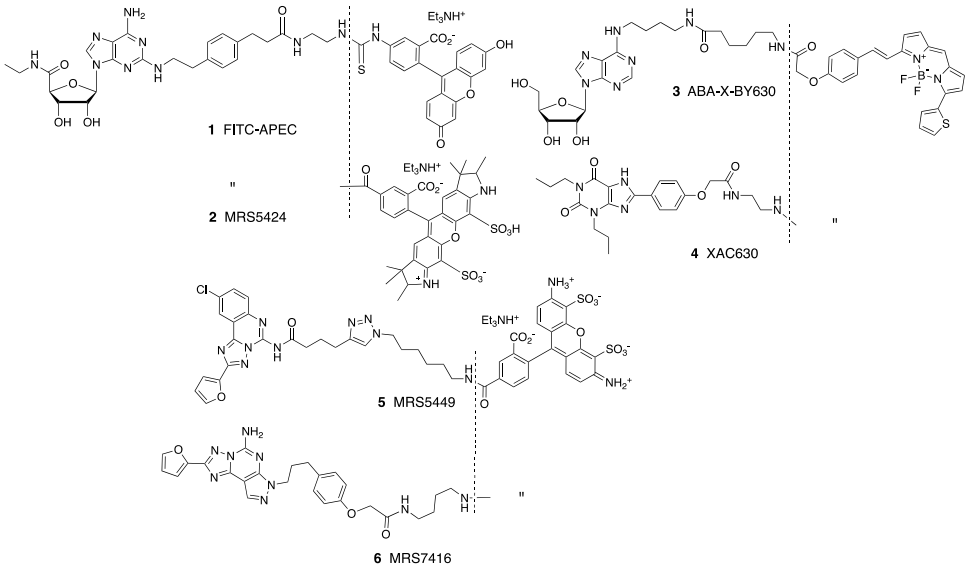

Fig. 1 Structures of six reported fluorescent agonists (**1**–**3**) and antagonists (**4**–**6**) for the ARs

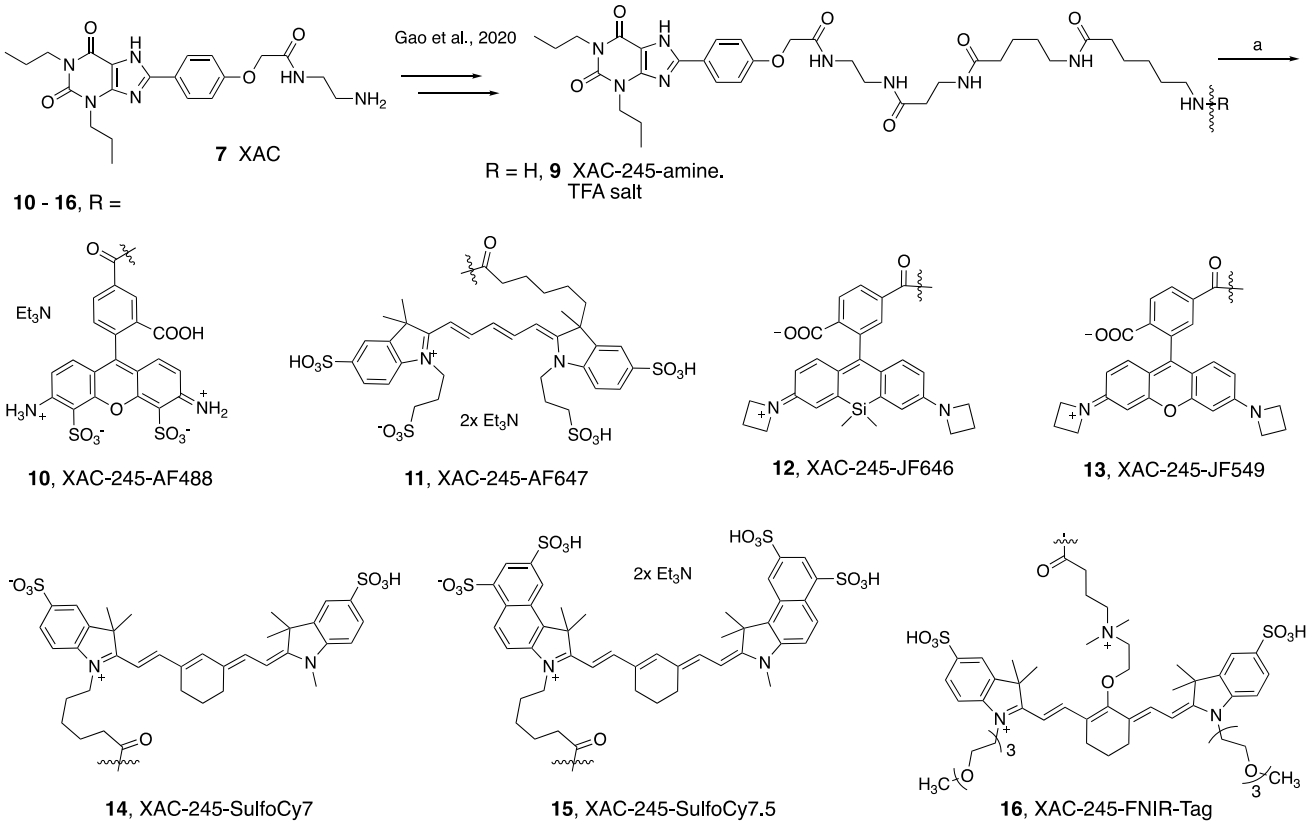

Scheme 1 Synthesis of XAC-fluorophore conjugates. *Reagents and conditions*: (a) functionalized fluorophore active ester (TFP or NHS), DMSO, DIPEA/TEA, rt in dark/wrapped in Al foil, 3–18 h, 40% to quantitative yields. Compound **9** was prepared as reported [13]

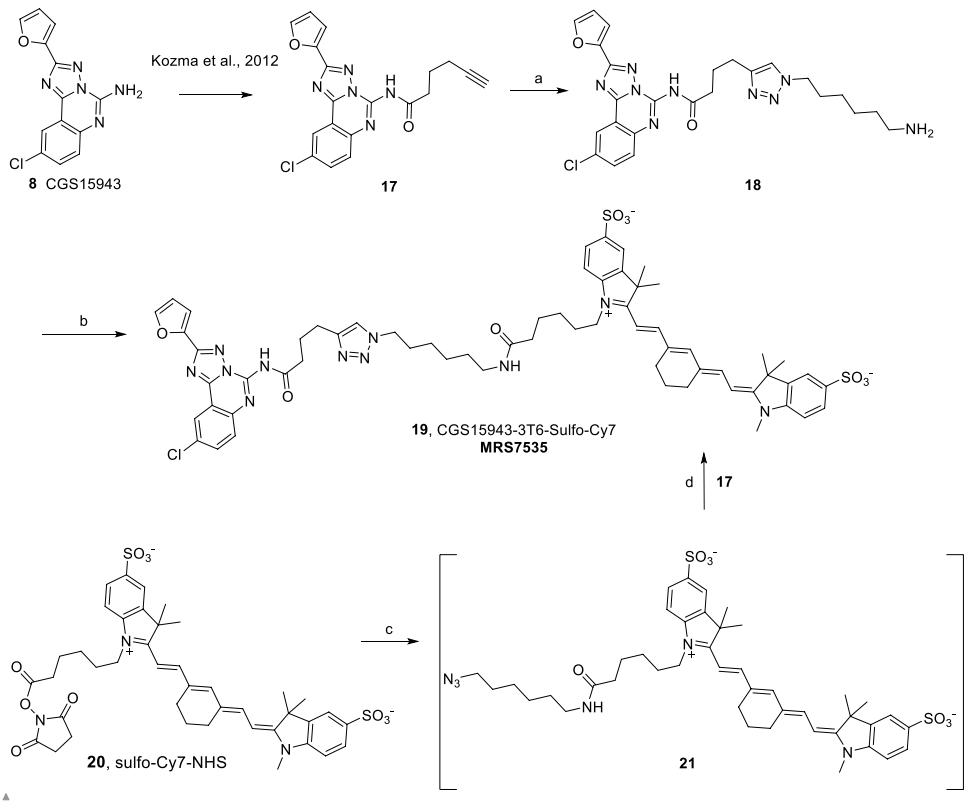

Scheme 2 Synthesis of CGS15943-derived fluorescent conjugate **19** by two routes. *Reagents and conditions*: (a) 6-azidohexan-1-amine, DMF, sodium ascorbate, $CuSO_4.5H_2O$, rt, 18 h, 6%; (b) DMSO, triethylamine, Sulfo-Cy7-NHS ester **20**, rt, 4 h, 24%. (c) 6-azidohexan-1-amine, DMF, rt, 4 h; (d) DMF, sodium ascorbate, $CuSO_4.5H_2O$, rt, 18 h, 5.3%. Compound **17** was prepared as reported [8]

distal modification of the functionalized chain. For example, xanthine derivative XAC-X-BY630 (CA200634) **4** and pyrazolo[4,3-e][1,2,4]triazolo[1,5-c]pyrimidin-5-amine derivative MRS7416 **6** each displayed negative cooperativity in A_{2A}AR binding [13]. A covalently binding fluorescent antagonist derived from A_{2A}AR antagonist ZM241385 was recently reported [15].

Since AR ligands are in development for various metabolic, neurological, inflammatory, and malignant conditions [16–21], additional AR fluorescent ligands are needed to expand the range of tool compounds for drug discovery. Here we conjugated known fluorophores to two known AR antagonist chemotypes, i.e., 1,3-dipropylxanthines aryl-functionalized at the C8 position and triazolo[1,5-c]quinazolin-5-yl) amines functionalized through acylation at the N^5 position [8, 22, 23]. These versatile scaffolds can be directed toward multiple AR subtypes based on their functionalization, and also dependent on the species being studied [24]. For example, 1,3-dialkyl-8-phenylxanthines, although originally reported as selective rat A_1AR antagonists [22], have been modified to achieve selectivity for the human (h) A_{2A}AR, A_{2B}AR, or A_3AR [24]. N-(2-Aminoethyl)-2-(4-(2,6-dioxo-1,3-dipropyl-2,3,6,7-tetrahydro-1*H*-purin-8-yl)phenoxy) acetamide (xanthine amine congener, XAC, **7**, Scheme 1) was designed to serve as a functionalized congener for coupling to reporter groups and carrier moieties [22] and served as a precursor here. A triazolo[1,5-c]quinazolin-5-yl)amine CGS15943 **8** (Scheme 2) binds to both A_{2A}AR and A_3AR and when acylated at the N^5 position can be highly selective for the hA_3AR (Scheme 2) [24]. In this study, we focus on the hA_{2A}AR and hA_3AR, using a wide range of tethered fluorophores, including the AlexaFluor (AF), JaneliaFluor (JF), cyanine, and near infrared (NIR) dyes [25, 26]. JF dyes, which are useful for super resolution microscopy and live cell imaging, do not photobleach as easily as other dyes, and some can be used for fluorescence detection of target protein binding without removing the supernatant [25]. The FNIR-Tag fluorophore was recently reported by Schnermann and coworkers as a tag for in vivo detection of NIR fluorescence [26].

Materials and methods

Chemistry

Materials and methods AF-dyes were purchased from Thermo Fisher Scientific (New York, USA); CGS15943 and JF dyes were from Tocris (Bio-techne, Minneapolis, MN, USA). Cyanine dyes were purchased from Lumiprobe (Cockeysville, MD, USA). All other chemicals and solvents were from Sigma-Aldrich (St. Louis, MO, USA). Anhydrous solvents were obtained directly from commercial sources. All reactions were carried out under argon atmosphere using anhydrous solvents. Room temperature or rt refers to 25 ± 2 °C. NMR spectra were recorded on a Bruker 400 MHz spectrometer. Chemical shifts are given in ppm (δ), calibrated to the residual solvent or TMS signals for hydrogen, carbon, and internally calibrated by solvent frequency for other nuclei (MestReNova 10.0.2). Exact mass measurements were performed on a proteomics optimized Q-TOF-2 (Micromass, Waters, Milford, MA, USA) mass spectrometer equipped with a standard electrospray ionization (ESI) and modular LockSpray TM interface. The RP-HPLC was performed using Luna 5 µm C18(2)100A, AXIA, 21.2 × 250 mm column (Phenomenex, Torrance, CA, USA). Purity was determined using C18-XDB, 5 µm, 4.6 × 250 mm column (Agilent, Santa Clara, CA, USA), and a 0 → 100% linear gradient of acetonitrile/10 mM triethylammonium acetate (TEAA) as mobile phase at flow rate of 1.0 mL/min. Purity of all the tested compounds was > 95% at 254 nm and/or the respective absorption wavelength in nm, unless noted otherwise.

Radioligands [^{3}H]cyclopentyl-1,3-dipropylxanthine ([^{3}H]DPCPX, 164 Ci/mmol), [^{3}H]-2-[*p*-(2-carboxyethyl) phenylethylamino]-5′-*N*-ethylcarboxamido-adenosine ([^{3}H]CGS21680, 30.5 Ci/mmol), and [^{125}I]N^6-(4-amino-3-iodobenzyl)adenosine-5′-*N*-methyluronamide ([^{125}I]I-AB-MECA, 2170 Ci/mmol) for A_1, A_{2A}, and A_3 receptors, respectively, were purchased from PerkinElmer (Waltham, MA, USA). DMEM medium and 1 M Tris–HCl (pH 7.5) were purchased from Mediatech, Inc. (Herndon, VA, USA). Adenosine deaminase was from Worthington Biochemical Corp. (Lakewood, NJ, USA). AR ligands 9-chloro-2-(2-furanyl)-[1,2,4]triazolo[1,5-c] quinazolin-5-amine (CGS15943) and CGS21680 were from Tocris (Ellisville, MO). XAC was synthesized at NIDDK, National Institutes of Health (Bethesda, MD). All other materials were from Sigma-Aldrich (St. Louis, MO, USA) or other standard commercial sources and of analytical grade. 6-Amino-*N*-(5-((3-((2-(2-(4-(2,6-dioxo-1,3-dipropyl-2,3,6,7-tetrahydro-1*H*-purin-8-yl)phenoxy) acetamido)ethyl)amino)-3-oxopropyl)amino)-5-oxopentyl) hexanamide (XAC245, **9**) was synthesized in the TFA salt form, as described in Gao et al. [13].

General procedure for the synthesis of XAC-fluorophore analogues (10–16)

A stock solution of XAC245.TFA (**9**, 6.0 mg, 7.26 µmol) and DIPEA (4.0 µL, 21.79 µmol) in anhydrous DMSO (596 µL) was prepared. To the TFP (2,3,5,6-tetrafluorophenyl)/NHS (*N*-hydroxysuccinimide)-ester of the fluorophore (1.0 eq.) was added XAC245.TFA-DIPEA-DMSO stock

solution (1.5 eq.) under argon atmosphere at room temperature. The reaction vial was covered with Al foil and stirred at room temperature for 18 h. The product was purified by C18-RP-HPLC.

10, XAC245-AF488 triethylamine salt Reacting AF488-5-TFP ester (1.0 mg, 1.13 µmol) with XAC245 stock solution (150 µL, 1.70 µmol) gave the product as an orange solid (0.88 mg, 59%, purified by RP-HPLC, linear gradient of CH_3CN-10 mM TEAA in H_2O (v/v) 05/95 → 45/55 in 40 min, flow rate = 5.0 mL/min, R_t = 39.14 min). ^1H NMR (400 MHz, D_2O) δ 8.20 (d, *J* = 1.9 Hz, 1H), 7.92 (dd, *J* = 7.9, 1.9 Hz, 1H), 7.72 (d, *J* = 8.5 Hz, 2H), 7.24 (d, *J* = 7.9 Hz, 1H), 6.98 (d, *J* = 9.3 Hz, 2H), 6.96–6.91 (m, 2H), 6.77 (d, *J* = 9.3 Hz, 2H), 4.53 (s, 2H), 3.98 (t, *J* = 7.5 Hz, 2H), 3.87 (t, *J* = 7.7 Hz, 2H), 3.47–3.33 (m, 5H), 3.29 (t, *J* = 6.8 Hz, 2H), 3.07 (t, *J* = 6.5 Hz, 2H), 2.32 (t, *J* = 6.8 Hz, 2H), 2.21 (t, *J* = 7.0 Hz, 2H), 2.05 (t, *J* = 7.2 Hz, 2H), 1.62 (dp, *J* = 15.8, 7.7 Hz, 8H), 1.51–1.33 (m, 7H), 0.89 (td, *J* = 7.4, 4.1 Hz, 6H). HRMS m/z $[M-H]^-$ for $C_{56}H_{65}O_{17}N_{11}S_2$ calculated 1226.3923, found 1226.3918.

11, XAC245-AF647 bis-triethylamine salt Reacting AF647-NHS ester (1.0 mg, 0.80 µmol) with XAC245 stock solution (130 µL, 1.60 µmol) gave the product as a blue-violet solid (1.80 mg, quantitative, purified by RP-HPLC, linear gradient of CH_3CN-10 mM TEAA in H_2O (v/v) 20/80 → 35/65 in 40 min, flow rate = 5.0 mL/min, R_t = 26.12 min). ^1H NMR (400 MHz, D_2O) δ 8.04–7.86 (m, 2H), 7.86–7.72 (m, 5H), 7.31 (d, *J* = 8.8 Hz, 1H), 7.24 (d, *J* = 8.4 Hz, 1H), 6.95 (d, *J* = 8.8 Hz, 2H), 6.42 (t, *J* = 12.4 Hz, 1H), 6.24 (d, *J* = 13.5 Hz, 1H), 6.13 (d, *J* = 13.5 Hz, 1H), 4.57 (s, 2H), 4.18 (s, 2H), 4.12 (t, *J* = 7.9 Hz, 2H), 3.97 (t, *J* = 7.6 Hz, 2H), 3.82 (t, *J* = 7.7 Hz, 2H), 3.45–3.28 (m, 6H), 3.06–2.89 (m, 9H), 2.36 (t, *J* = 6.8 Hz, 2H), 2.17 (dt, *J* = 19.4, 7.4 Hz, 2H), 2.11–2.04 (m, 3H), 2.01 (t, *J* = 7.2 Hz, 2H), 1.68 (q, *J* = 7.6 Hz, 2H), 1.65–1.56 (m, 9H), 1.56–1.49 (m, 1H), 1.40 (dp, *J* = 21.8, 7.3 Hz, 4H), 1.14 (dt, *J* = 17.1, 8.0 Hz, 3H), 0.89 (dt, *J* = 18.6, 7.4 Hz, 6H). HRMS m/z $[M-H]^-$ for $C_{71}H_{97}O_{20}N_{11}S_4$ calculated 1550.5716, found 1550.5736.

12, XAC245-JF646 Reacting JF646-NHS ester (1.0 mg, 1.70 µmol) with XAC245 stock solution (210 µL, 2.5 µmol) gave the product as a light blue solid (1.0 mg, 50%, purified by RP-HPLC, linear gradient of CH_3CN-10 mM TEAA in H_2O (v/v) 50/50 → 100/00 in 40 min, flow rate = 5.0 mL/min, R_t = 32.32 min). ^1H NMR (400 MHz, DMSO-d_6) δ 8.73 (t, *J* = 5.6 Hz, 1H), 8.17 (t, *J* = 5.6 Hz, 1H), 8.11–7.97 (m, 3H), 7.93 (t, *J* = 5.5 Hz, 1H), 7.77 (t, *J* = 5.7 Hz, 1H), 7.70 (t, *J* = 5.6 Hz, 1H), 7.66 (s, 1H), 7.01 (d, *J* = 8.3 Hz, 2H), 6.71 (d, *J* = 2.7 Hz, 2H), 6.62 (d, *J* = 8.7 Hz, 2H), 6.32 (dd, *J* = 8.7, 2.7 Hz, 2H), 4.50 (s, 2H), 3.98 (t, *J* = 7.3 Hz, 2H), 3.83 (q, *J* = 7.0 Hz, 10H), 3.18 (ddt, *J* = 18.0, 11.3, 6.3 Hz, 7H), 2.97 (q, *J* = 6.5 Hz, 2H), 2.42 (q, *J* = 7.1 Hz, 2H), 2.29 (p, *J* = 7.3 Hz, 4H), 2.20 (t, *J* = 7.0 Hz, 2H), 2.01 (td, *J* = 7.4, 2.4 Hz, 4H), 1.72 (q, *J* = 7.4 Hz, 2H), 1.55 (q, *J* = 7.4 Hz, 2H), 1.43 (dq, *J* = 14.5, 7.2 Hz, 5H), 1.36–1.15 (m, 8H), 0.97–0.79 (m, 9H), 0.60 (s, 3H), 0.49 (s, 3H). HRMS m/z $[M+H]^+$ for $C_{64}H_{79}O_{10}N_{11}Si$ calculated 1190.5859, found 1190.5859.

13, XAC245-JF549 Reacting JF549-NHS ester (1.15 mg, 2.10 µmol) with XAC245 stock solution (260 µL, 3.15 µmol) gave the product as a dark pink solid (0.83 mg, 40%, purified by RP-HPLC, linear gradient of CH_3CN-10 mM TEAA in H_2O (v/v) 05/95 → 95/05 in 40 min, flow rate = 5.0 mL/min, R_t = 30.10 min). ^1H NMR (400 MHz, DMSO-d_6) δ 8.69 (s, 1H), 8.15 (d, *J* = 9.9 Hz, 2H), 8.07–7.89 (m, 3H), 7.78 (s, 1H), 7.70 (s, 1H), 7.63 (s, 1H), 6.98 (s, 2H), 6.56 (s, 1H), 6.50 (d, *J* = 8.6 Hz, 1H), 6.21 (d, *J* = 2.2 Hz, 2H), 6.19–6.10 (m, 2H), 4.48 (s, 2H), 3.97 (s, 2H), 3.85 (t, *J* = 7.3 Hz, 9H), 3.67 (d, *J* = 11.0 Hz, 1H), 3.27–3.06 (m, 40H), 2.96 (d, *J* = 6.6 Hz, 2H), 2.42 (q, *J* = 7.1 Hz, 2H), 2.37–2.24 (m, 3H), 2.19 (t, *J* = 7.0 Hz, 2H), 2.00 (d, *J* = 6.5 Hz, 4H), 1.72 (d, *J* = 7.8 Hz, 2H), 1.54 (d, *J* = 7.1 Hz, 1H), 1.43 (s, 5H), 1.36–1.11 (m, 6H), 1.00–0.77 (m, 10H). HRMS m/z $[M+H]^+$ for $C_{62}H_{73}N_{11}O_{11}$ calculated 1148.5569, found 1148.5585.

14, XAC245-Sulfo-Cy7 Reacting Sulfo-Cy7-NHS ester (1.06 mg, 1.26 µmol) with XAC245 stock solution (156 µL, 1.90 µmol) gave the product as a blue solid (1.61 mg, 91%, purified by RP-HPLC, linear gradient of CH_3CN-10 mM TEAA in H_2O (v/v) 05/95 → 100/00 in 40 min, flow rate = 5.0 mL/min, R_t = 27.36 min). ^1H NMR (400 MHz, DMSO-d_6) δ 8.22 (s, 1H), 8.11–8.04 (m, 2H), 7.97 (d, *J* = 5.7 Hz, 1H), 7.83–7.66 (m, 4H), 7.62 (ddd, *J* = 9.7, 5.5, 2.7 Hz, 1H), 7.28 (dd, *J* = 13.1, 8.3 Hz, 1H), 7.09 (d, *J* = 8.9 Hz, 2H), 6.53 (s, 1H), 6.14 (dd, *J* = 14.2, 6.8 Hz, 2H), 4.54 (s, 2H), 4.10 (s, 2H), 4.01 (t, *J* = 7.3 Hz, 2H), 3.92–3.81 (m, 2H), 3.61 (s, 3H), 3.25–3.07 (m, 5H), 2.96 (q, *J* = 6.4 Hz, 4H), 2.20 (t, *J* = 7.1 Hz, 2H), 2.10–1.95 (m, 6H), 1.88–1.70 (m, 3H), 1.65 (d, *J* = 3.2 Hz, 10H), 1.56 (dq, *J* = 14.0, 7.2 Hz, 2H), 1.48–1.38 (m, 2H), 1.25–1.10 (m, 2H), 1.04 (q, *J* = 7.8, 7.3 Hz, 6H), 0.88 (dt, *J* = 11.3, 7.4 Hz, 6H). HRMS m/z $[M+H]^+$ for $C_{72}H_{95}O_{14}N_{11}S_2$ calculated 1402.6580, found 1402.6597.

15, XAC245-Sulfo-Cy7.5 Reacting Sulfo-Cy7.5-NHS ester (1.4 mg, 1.20 µmol) with XAC245 stock solution (150 µL, 1.80 µmol) gave the product as a blue solid (1.52 mg, 69%, purified by RP-HPLC, linear gradient of CH_3CN-10 mM TEAA in H_2O (v/v) 05/95 → 45/55 in 40 min, flow rate = 5.0 mL/min, R_t = 38.58 min). ^1H NMR (400 MHz, D_2O) δ 8.72 (dd, *J* = 14.2, 9.1 Hz, 2H), 8.56 (d, *J* = 11.4 Hz, 2H), 8.31 (d, *J* = 8.4 Hz, 1H), 7.48 (dt, *J* = 30.3, 14.5 Hz, 3H), 7.34 (d, *J* = 8.2 Hz, 2H), 7.06 (s, 1H), 6.57 (d, *J* = 8.3 Hz,

2H), 5.79 (dd, J = 28.7, 13.8 Hz, 2H), 4.34 (s, 2H), 3.92–3.65 (m, 6H), 3.53–3.28 (m, 9H), 3.03 (t, J = 6.8 Hz, 2H), 2.73 (d, J = 12.4 Hz, 2H), 2.40 (t, J = 6.8 Hz, 2H), 2.27–2.04 (m, 8H), 1.96 (t, J = 7.5 Hz, 2H), 1.74 (s, 12H), 1.46 (s, 8H), 1.39–1.31 (m, 1H), 1.12 (s, 1H), 0.94 (d, J = 8.5 Hz, 1H), 0.80 (dt, J = 15.2, 7.2 Hz, 8H). HRMS m/z $[M+H]^+$ for $C_{80}H_{97}O_{20}N_{11}S_4$ calculated 1660.5872, found 1660.5852.

16, XAC245-FNIR-Tag Reacting FNIR-Tag-NHS ester (0.5 mg, 0.43 µmol) with XAC245 stock solution (55 µL, 0.65 µmol) gave the product as a green solid (0.53 mg, 70%, purified by RP-HPLC, linear gradient of CH_3CN-10 mM TEAA in H_2O (v/v) 05/95 → 65/35 in 40 min, flow rate = 5.0 mL/min, R_t = 36.35 min). ^{1}H NMR (400 MHz, DMSO-d_6) δ 8.17 (s, 1H), 7.95 (t, J = 13.0 Hz, 5H), 7.80 (s, 2H), 7.74 (t, J = 5.6 Hz, 1H), 7.63 (d, J = 8.1 Hz, 1H), 7.33 (d, J = 8.4 Hz, 2H), 6.94 (d, J = 8.6 Hz, 2H), 6.28 (d, J = 14.1 Hz, 2H), 4.46 (s, 2H), 4.36 (d, J = 6.7 Hz, 3H), 3.99 (d, J = 25.1 Hz, 3H), 3.80 (dt, J = 10.4, 6.3 Hz, 5H), 3.65 (s, 1H), 3.51 (dd, J = 5.9, 3.5 Hz, 4H), 3.22 (s, 4H), 3.18 (s, 3H), 3.10–3.02 (m, 1H), 2.97 (d, J = 6.2 Hz, 1H), 2.58 (s, 3H), 2.42 (q, J = 7.1 Hz, 14H), 2.21 (q, J = 7.1 Hz, 3H), 2.05–1.96 (m, 5H), 1.86 (s, 13H), 1.68 (s, 10H), 1.53 (d, J = 7.1 Hz, 1H), 1.43 (s, 4H), 1.34–1.16 (m, 5H), 0.93 (t, J = 7.1 Hz, 20H), 0.86 (dd, J = 14.1, 7.2 Hz, 6H). HRMS m/z $[M+H]^+$ for $C_{88}H_{128}O_{21}N_{12}S_2$ calculated 1753.8837, found 1753.8864.

18, CGS15943-3T6-amine To a suspension of compound **17** [8] (20 mg, 0.053 mmol) in DMF (1.0 mL) was added sequentially a freshly prepared solution of sodium ascorbate (1 M, 132 µL, 0.132 mmol), 6-azidohexane-1-amine [27] (15 mg, 0.106 mmol) and $CuSO_4.5H_2O$ (1 M, 27 µL, 0.027 mmol) and the mixture stirred at room temperature for 18 h. The solvent was evaporated under high vacuum, and the residue was purified by silica-gel column chromatography to afford the **18** as a minor product (1.5 mg, 6%; R_f = 0.3, TLC eluent = 10% MeOH in CH_2Cl_2 + 1% Et_3N). ^{1}H NMR (400 MHz, DMSO) δ 8.16 (dd, J = 8.0, 2.6 Hz, 1H), 7.97–7.78 (m, 2H), 7.75–7.63 (m, 1H), 7.56 (d, J = 8.8 Hz, 1H), 7.21 (d, J = 3.8 Hz, 1H), 6.71 (s, 1H), 4.33–4.17 (m, 2H), 2.69 (t, J = 8.7 Hz, 2H), 2.63–2.51 (m, 2H), 1.92 (t, J = 7.4 Hz, 2H), 1.82–1.65 (m, 2H), 1.44–1.11 (m, 6H). HRMS m/z $[M+H]^+$ for $C_{25}H_{28}O_2N_9Cl$ calculated 522.2133, found 522.2134.

19, CGS15943-3T6-Sulfo-Cy7

First route

A mixture of compound **18** (1.5 mg, 2.87 µmol) and triethylamine (2.0 µL, 14.0 µmol) in anhydrous DMSO (150 µL) was added to Sulfo-Cy7-NHS ester **20** (1.0 mg, 1.20 µmol) under insert atmosphere and stirred at room temperature for 4 h. The product was purified immediately by RP-HPLC to afford compound **19** as a dark-blue solid (0.34 mg, 24%; purified using Agilent C18-XDB 4.6 × 250 mm column and linear gradient of CH_3CN/10 mM aq. TEAA (v/v) 20/80 → 55/45 in 20 min at 1.00 mL/min, R_t = 17.34 min). ^{1}H NMR (400 MHz, DMSO) δ 8.39 (s, 1H), 8.00 (s, 1H), 7.91 (s, 2H), 7.75 (s, 3H), 7.61–7.33 (m, 4H), 7.25–7.34 (m, 3H), 6.77 (s, 1H), 6.52 (s, 1H), 6.11–6.19 (m, 2H), 4.28 (t, J = 7.4 Hz, 2H), 4.09 (m, 2H), 3.61 (s, 3H), 2.94 (m, 6H), 2.67–2.77 (m, 4H), 1.91–2.02 (m, 4H), 1.78 (m, 2H), 1.65 (s, 8H), 1.52 (m, 2H), 1.13–1.31 (m, 6H), 1.12 (t, J = 7.1 Hz, 4H). HRMS m/z $[M-H]^-$ for $C_{62}H_{70}O_9N_{11}S_2Cl$ calculated 1210.4410, found 1210.4409. Purity—94.69% at 750 nm; 88.20% at 254 nm.

Second route

To a solution of compound **20** (100 mM, 13 µL, 0.013 mmol) in DMF was added 6-azidohexan-1-amine (100 mM, 15 µL, 0.015 mmol) and the mixture stirred at room temperature for 4 h. The reaction mixture was evaporated under a stream of nitrogen gas. Freshly prepared solution of sodium ascorbate (50 mM, 158 µL, 0.079 mmol), $CuSO_4$•$5H_2O$ (50 mM, 30 µL, 0.015 mmol), and compound **17** (100 mM, 32 µL, 0.032 mmol) were added and the mixture stirred at room temperature for 18 h. The product was purified by RP-HPLC, using the same conditions as above, to afford compound **19** as a dark-blue solid (1.96 mg, 5.3%).

To avoid freeze–thaw cycles, compound **19** was dissolved in EtOH and divided into small aliquots that were dried and stored at − 80 °C for use in binding assays. Radioligand binding was performed as described in Gao et al. [13].

Flow cytometry

Saturation assay: determination of dissociation constant

Flow cytometry was run using a CytoFLEX B4-RO-VO System (Beckman Coulter, Brea, CA, USA). The instrument includes 13 band pass filters which can be repositioned as needed, and it is available with different configurations to provide application flexibility. Violet side scatter resolution: (VSSC) < 200 nm blue laser wavelength: 488 nm; power: 50 mw; beam spot size: 5 × 80 µm; red laser wavelength: 638 nm; power: 50 mw; beam spot size: 5 × 80 µm; violet laser wavelength: 405 nm; power: 80 mw; beam spot size: 5 × 80 µm; flow cell dimensions: 420 µm × 180 µm internal diameter; signal processing: fully digital system with a 7-decade data display; carryover: single tube format < 1.0%; plate loader format < 0.5%.

HEK293 cells expressing either human A_3AR or human A_{2A}AR were plated in black 96-well plates overnight in complete DMEM media (DMEM, FBS (10%), penicillin/steptomycin (100 U/mL)). Media was then aspirated, and

fresh complete media containing a range of concentrations of fluorescent ligand was added to appropriate cells. Non-specific binding was prepared through the addition of XAC (14 µM final concentration) at each concentration of fluorescent ligand. Cells were incubated for 1 h at 37 °C. Media was then aspirated, and cells were detached with non-enzymatic Cellstripper and resuspended in 200 µL PBS (without Ca^{2+}, Mg^{2+}). Cell fluorescence was measured on a CytoFLEX B4-RO-VO system. For the detection of **19** and **12**, a 638-nm laser was employed and a 780/60 bandpass filter and a 660/20 bandpass filter were used, respectively. The data were analyzed using CellQuest Software. Specific binding was calculated by subtracting non-specific binding from total binding.

Competitive binding assay

For competitive binding experiments, chemically transfected HEK293 cells expressing either human A_3AR or human A_{2A}AR were plated in black 96-well plates overnight in complete DMEM media (DMEM, FBS (10%), penicillin/streptomycin (100 U/mL)). The media was then aspirated and increasing concentrations of ligand in complete DMEM media were incubated with **12** (250 nM) for hA_{2A}AR or **19** (100 nM) for hA_3AR expressing cells at 37 °C for 1 h. XAC (14 uM) was used to determine non-specific binding. Media was then aspirated, and cells were detached with non-enzymatic Cellstripper and resuspended in PBS (without Ca^{2+}, Mg^{2+}). Cell fluorescence was measured on a Beckman Coulter CytoFLEX B4-RO-VO system. For the detection of **19** and **12**, a 638-nm laser was employed and a 780/60 bandpass filter and a 660/20 bandpass filter were used, respectively. The data were analyzed using CellQuest Software. Specific binding was calculated by subtracting non-specific binding from total binding. The inhibition constants (K_i), dissociation constants (K_d), and kinetic constants were calculated using Prism, version 9.0.0 (GraphPad, San Diego, CA).

Determination of off-rate

Chemically transfected HEK293 cells expressing human A_3AR were plated in black 96-well plates overnight in complete DMEM media (DMEM, FBS (10%), penicillin/streptomycin (100 U/mL)). Media was then aspirated, and fresh complete media containing a saturating concentration of **19** (400 nM) was added to each well. Cells were then incubated for 1 h at 37 °C. Media was then aspirated and PBS (without Ca^{2+}, Mg^{2+}) containing a saturating concentration of XAC (100 µM) was added to each well. Upon addition of XAC, data collection immediately began and continued for various timepoints using a Beckman Coulter CytoFLEX B4-RO-VO system with a 638-nm red laser and a 780/60 bandpass filter. Dissociation of **19** was followed by the change in mean fluorescence intensity (MFI) vs time. Data were analyzed using CellQuest Software.

The laser wavelengths of the longpass/bandpass filters used for the flow cytometry experiment were not optimal for compound **19**. The λ_{max} of the Sulfo-Cy7 fluorophore of **19** is 750 nm. Therefore, the 638-nm laser used to excite **19** resulted in low fluorescence emission consistent with non-optimal excitation. However, the emission signal resulting from the 638-nm excitation was sufficient to obtain a signal.

Confocal microscopy

HEK293 cells transiently expressing human A_{2A}AR were plated in 8-well Ibibi µ-slides and grown overnight in complete DMEM media (DMEM, FBS (10%), containing penicillin/streptomycin (100 U/mL)). The media was removed, and total binding was determined by treatment of cells with 500 nM **12** in complete DMEM media. Non-specific binding was determined by cotreatment of cells with 500 nM **12** and 50 µM XAC. Cells were incubated with treatments for 1 h. Media was removed and DPBS (w/Ca^{2+} & Mg^{2+}) was added.

Cell fluorescent imaging

A Zeiss LSM 700 confocal scanhead (Carl Zeiss Microscopy, LLC, Thornwood, NY, USA) mounted on a Zeiss AxioObserver. Z1 microscope, running ZEN 2.3 software, was used to simultaneously collect brightfield with fluorescence overlay images. The objective lens used was the Zeiss Plan-Apo 63×/1.4 Oil DIC. The 639-nm laser was used for illumination/excitation, at 28.4% power. Emission was filtered by a 640-nm longpass filter. Imaging was set at a scan field of 203.12 µm×203.12 µm with a pinhole of 61 µm, which corresponds to a confocal sectioning thickness of 1.0 µ.

Molecular modeling

The model of hA_3AR was retrieved from a previous work [28], where it was obtained through homology modeling using an antagonist-bound inactive structure of hA_1AR (PDB ID: 5UEN [29]) as a template, minimization of non-conserved residues and induced fit docking of the high affinity A_3AR antagonist *N*-[9-chloro-2-(2-furanyl)[1,2,4]triazolo[1,5-c] quinazolin-5-yl]benzeneacetamide (MRS1220).

The structure was prepared with the Protein Preparation Wizard tool [30] (Schrödinger suite, Maestro 2021–2 [31], New York, NY, USA). The predicted tautomeric state of histidines was HIE (hydrogen at Nε nitrogen) for H79, H95, H124, H158 and H304, and HID (hydrogen at Nδ nitrogen) for H272.

Compound **19** was docked at the receptor orthosteric binding site using Glide-XP [32–34], employing a grid centered on

the centroid of F168 and N250, and with inner and outer box dimensions of 10 Å and 46 Å, respectively. The conformational search was restricted constraining the scaffold of compound **9** to the reference pose of MRS1220, using the maximum common substructure option and an RMSD tolerance of 2 Å. A maximum of 20 poses was set as output, and a post-docking minimization phase was included. One pose was generated.

Results

Chemistry To prepare various fluorescent compounds for this study, derivatives of XAC **7** and CGS15943 **8** with a linker containing a primary amine group were prepared and coupled with respective chromophores (Schemes 1 and 2). XAC245-amine TFA salt **9** was synthesized by successive addition of *N*-Boc-amino acids as reported earlier [13]. The pharmacologically active XAC-fluorophore conjugates **10**–**16** were synthesized by the reaction of corresponding amines with activated fluorophore esters under basic conditions (Scheme 1). Cyanine dyes appear in compound **11** and NIR probes **14**–**16**. The two JF dye conjugates containing azetidine moieties are **12** (JF649) and **13** (JF549). Compound **16** contains a net neutral heptamethine cyanine with a stable C4′-*O*-alkyl linker as reported [26]. This fluorophore has a λ_{max} of 765 nm, with emission at 788 nm. Sulfo-Cy7 conjugate **19** has a λ_{max} of ~ 750 nm, with emission at ~ 773 nm. The spectral characteristics of each fluorophore are given in Supporting Information.

For the synthesis of an **8**-derived fluorescent compound **19**, a click reaction between alkyne **17** [8] and an azide [27] gave the product **18** in low yields (Scheme 2). The reaction had unreacted starting material **17** and the major by-product **8**, both of which were recovered. An amide bond formation by the amino group in compound **18** with activated carbonyl of Sulfo-Cy7-NHS ester **20** gave the desired product CGS15943-3T6-Sulfo-Cy7 **19** in acceptable yields. A second, more efficient route involved the coupling of the fluorophore as an active ester **20** to 6-azidohexan-1-amine, followed by click reaction of the resulting azide **21** to the alkyne-functionalized pharmacophore **17**. The overall yield of the second route (compound **19** compared to the amount of compound **17**) was ~ tenfold higher than the first route.

Affinity determination The AR affinity of the fluorescent derivatives was initially determined using standard radioligand binding methods [10, 13] in membranes of

Table 1 Fluorescent ligand binding affinities[a] at three AR subtypes

No	Compound	*h*A_1, K_i (nM) or % inhib. at 1 μM	*h*A_{2A} K_i (nM) or % inhib. at 1 μM	*h*A_3 K_i (nM) or % inhib. at 1 μM
XAC **7** and its conjugates				
7	XAC[b]	8.3 ± 1.1	32.1 ± 5.9	38.3 ± 6.7
9	XAC-245[b]	*35%*	198 ± 33	220 ± 36
10	XAC245-AF488	*19%*	316 ± 24	*40 ± 3%*
11	XAC245-AF647	*18%*	*37 ± 21%*	*41 ± 5%*
12	XAC245-JF646[c]	*53%*	144 ± 24	495 ± 89
13	XAC245-JF549	*29%*	882 ± 215	*36.9 ± 4.3%*
14	XAC245-Sulfo-Cy7 (750 nm)[d]	*20%*	1290 ± 470	*49.7 ± 11.8%*
15	XAC245-Sulfo-Cy7.5 (778 nm)[d]	*27%*	1120 ± 310	*30.8 ± 3.5%*
16	XAC245-FNIR-Tag (765 nm)[d]	*27%*	956 ± 232	232 ± 53
CGS15943 **8** and its conjugates				
8	CGS15943[e]	3.5	1.2	35
5	MRS5449[e]	87 ± 24	73 ± 8	6.4 ± 2.5
17	Alkyne deriv.[e]	170 ± 40	51 ± 10	33.5 ± 10.1
19	CGS15943-3T6-Sulfo-Cy7[c]	*53%*	244	21.6 ± 4.0

[a]Determined with membranes of HEK293 cell expressing each receptor and using the following radioligands (final concentration in incubation medium), unless noted: A_1, [^{3}H]DPCPX (0.7 nM); A_{2A}, [^{3}H]CGS21680 (8.1 nM); A_3, [.^{125}I]I-AB-MECA (0.15 nM). Results are expressed as mean ± SEM from at least 3 independent experiments

[b]A_{2A} and A_3 AR affinities reported in Gao et al. [13]. A_1AR affinity of XAC (using [^{3}H]R-PIA) is from Kecskés et al. [46]

[c]**12**, MRS7774; **19**, MRS7535

[d]Excitation wavelength

[e]AR affinities reported in Kozma et al. [8]

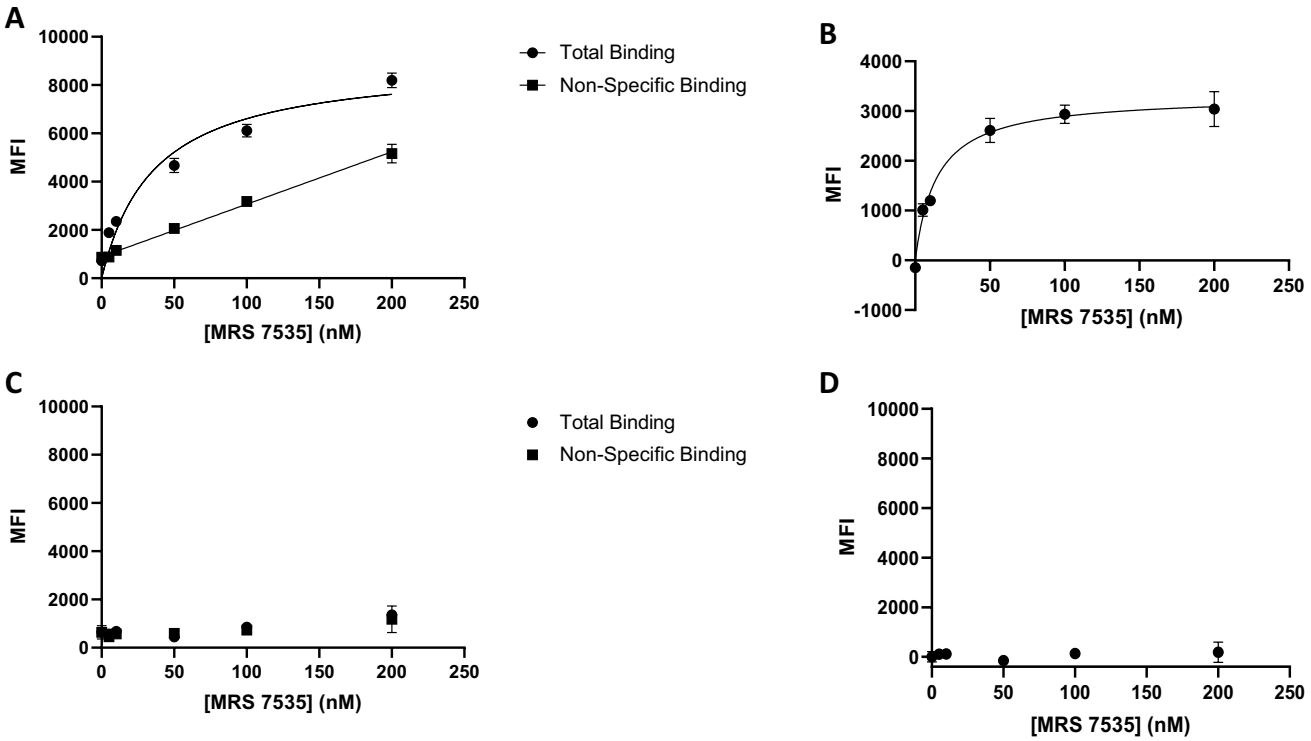

Fig. 2 Representative saturation binding assay with **19** using FCM in HEK293 cells expressing hA_3AR (A, B) or non-transfected HEK293 cells (C, D), $N = 2$ for all experiments. Fluorescence intensity was measured using a Beckman Coulter CytoFLEX B4-RO-VO System with a 638-nm laser and a 780/60 bandpass filter. (A) Total binding of HEK293 cells expressing hA_3AR was determined by treating cells with a range of concentrations of **19,** and non-specific binding was determined in the presence of XAC (14 μM). (B) Specific binding of **19** at HEK293 cells expressing hA_3AR, calculated as total binding MFI minus non-specific binding MFI. The dissociation constant (K_d) was calculated to be 11.8 ± 0.7 nM. Results reported as mean ± SEM. Note that the Y-axis in (B) has a different scale compared to other plots. (C) Total and nonspecific binding of **19** with non-transfected HEK293 cells. (D) Lack of specific binding of **19** with non-transfected HEK293 cells

HEK293 cells overexpressing each receptor: A_1, A_{2A}, and A_3 (Table 1). The highest affinity was observed for the fluorescent conjugates **10**, **12**, and **19** at the $A_{2A}AR$ (K_i 144–316 nM). The A_1AR affinity was generally low ($K_i > 1$ μM) and only percent inhibition is indicated. The A_3AR and $A_{2A}AR$ affinities were consistently higher than at the A_1AR with the highest A_3AR affinity (K_i 21.6 nM) observed for **19**. Compounds **10** and **13–15** were inactive at the A_3AR. Thus, compound **12** was highly selective for the $A_{2A}AR$ compared to the A_1AR, but only 3.4-fold selective compared to A_3AR. Compounds **13–15** were > two-fold selective for the $A_{2A}AR$ compared to the A_3AR. Binding affinity was measured for two compounds at the $hA_{2B}AR$, using [^{3}H]8-cyclopentyl-1,3-dipropylxanthine ([^{3}H]DPCPX) as radioligand in membranes of transfected HEK293 cells [28]. At a concentration of 1 μM, compounds **12** and **19** inhibited binding by only 57.1% and 38.5%, respectively. Thus, these two fluorescent ligands were selective for their respective target receptors compared to the $A_{2B}AR$.

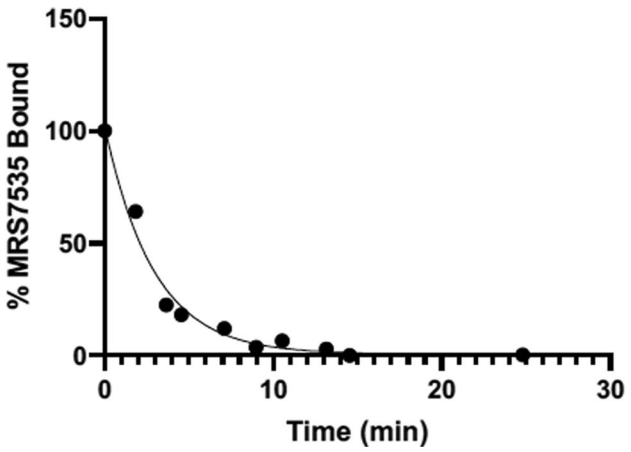

Fig. 3 Kinetic determination of k_{off} for **19** at hA_3AR in HEK293 cells expressing hA_3AR ($N = 2$). Cells were treated with a saturating concentration of **19** (400 nM) in complete DMEM media and incubated for 1 h at 37 °C. Media was removed, and PBS (without Ca^{2+}, Mg^{2+}) containing XAC (100 μM) was added to the cells. MFI was measured over time. Data were fit to a monophasic decay curve. Apparent k_{off} was measured to be 0.334 min^{-1} ($N = 1$). Results reported as mean ± SEM

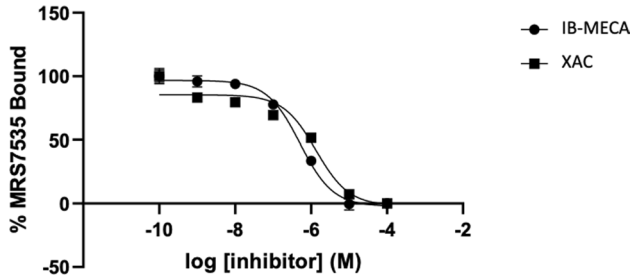

Fig. 4 Competitive binding of **19** with a non-selective antagonist, XAC, and an A_3AR-selective agonist, IB-MECA, in HEK293 cells expressing hA_3AR determined using FCM. Fluorescence intensity was measured using a Beckman Coulter CytoFLEX B4-RO-VO System with a 638-nm laser and a 780/60 bandpass filter. A K_i of 171 ± 29 nM ($N = 2$) was calculated for XAC and 71 ± 17 nM ($N = 2$) for IB-MECA based on a K_d of 11.8 nM for **19** at $hA_{2A}AR$

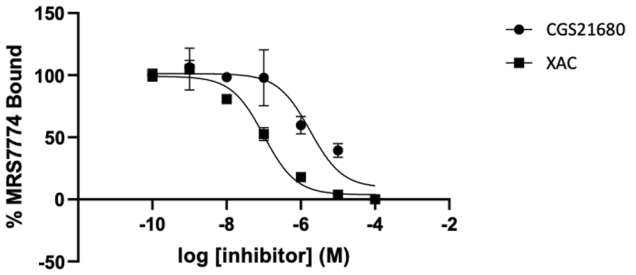

Fig. 6 Competitive binding of **12** with antagonist, XAC and A_{2A}AR-selective agonist, CGS21680 in HEK293 cells expressing $hA_{2A}AR$. Fluorescence intensity was measured using a Beckman Coulter CytoFLEX B4-RO-VO System with a 638-nm laser and a 660/20 bandpass filter. A K_i of 53 ± 6 nM (N = 2) was calculated for XAC and 783 ± 52 nM (N = 2) for CGS21680 based on a K_d of 222 nM for **12** at $hA_{2A}AR$

Application to flow cytometry and fluorescence microscopy The objective was to determine the suitability of these fluorescent conjugates for use in binding assays by flow cytometry and in fluorescence microscopy. The conjugate with the highest A_3AR affinity was compound **19** , with a radioligand binding K_i value of 21.6 nM. The fluorophore of **19** was a NIR dye with a maximum excitation wavelength of 750 nm, which could be sufficiently exited with a red laser (638 nm) to obtain significant emission due to the high quantum yield (0.88) of the dye. A saturation experiment (Fig. 2) using human embryonic kidney (HEK) 293 cells overexpressing the A_3AR indicated an acceptably low level of non-specific binding (determined using 14 μM XAC). Non-specific binding was linear with respect to the fluorescent ligand concentration (up to 200 nM). The specific binding of **19** was saturable up to a concentration of 200 nM. A K_d value of 11.8 ± 0.7 nM was determined by nonlinear regression analysis using a one-site specific binding model (Eq. 1: $y = B_{max} * x/(K_d + x)$. In non-AR-expressing control HEK293 cells, specific binding of **19** was absent.

Kinetic experiments showed the off-rate to be 0.0118 nM^{-1} min^{-1} (Fig. 3), while the on-rate calculated from binding saturation K_d and k_{off} was 0.334 min^{-1} ($N = 1$).

Fluorescent binding inhibition (Fig. 4) by known A_3AR agonist IB-MECA and AR antagonist XAC was performed using a fixed concentration of **19** (100 nM) resulting in sigmoidal inhibition curves with Hill coefficients ~ 1. This high concentration (~ 10X the K_d of **19**) was needed to obtain an adequate signal. The K_i values of 71 and 171 nM for IB-MECA and XAC, respectively, were of the same rank order, but roughly an order of magnitude higher than radioligand binding K_i values obtained for the same ligands at the hA_3AR. Their reported K_i values using an A_3AR agonist radioligand were 1.8 and 13.8, respectively [8].

A_{2A}AR flow cytometry (Fig. 5 and Fig. 6) and microscopic cell imaging data (Fig. 7) were determined using the conjugate **12** showing the highest A_{2A}AR affinity. A FCM binding saturation experiment demonstrated a K_d value of 222 nM at the $hA_{2A}AR$ by Scatchard analysis, which is close to its binding K_i value in Table 1. Competition for

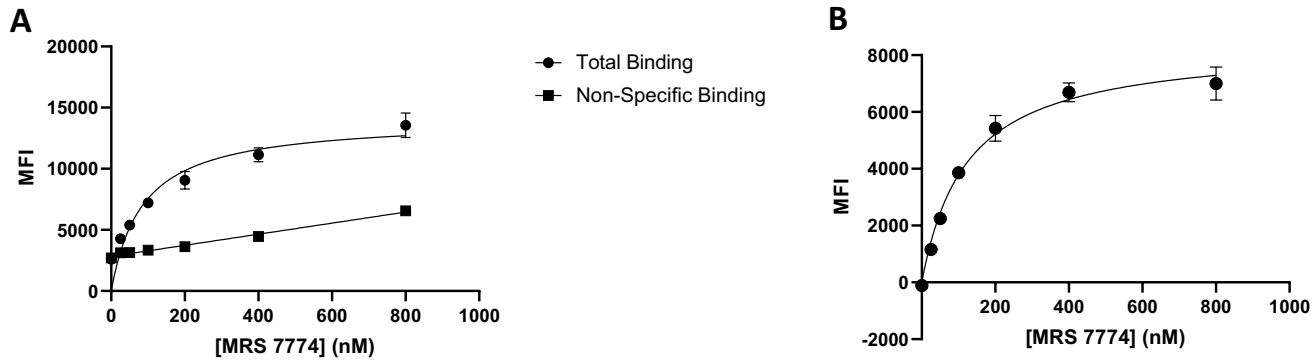

Fig. 5 Representative saturation binding assay with **12** using FCM in HEK293 cells expressing $hA_{2A}AR$. Fluorescence intensity was measured using a Beckman Coulter CytoFLEX B4-RO-VO System with a 638-nm laser and a 660/20 bandpass filter. (A) Total binding of HEK293 cells expressing $hA_{2A}AR$ was determined by treating cells with a range of concentrations of **12** and non-specific binding determined in the presence of XAC (14 μM). (B) Specific binding of **12** at HEK293 cells expressing $hA_{2A}AR$, calculated as total binding MFI minus non-specific binding MFI. The dissociation constant (K_d) was determined to be 222 ± 64 nM ($N = 3$)

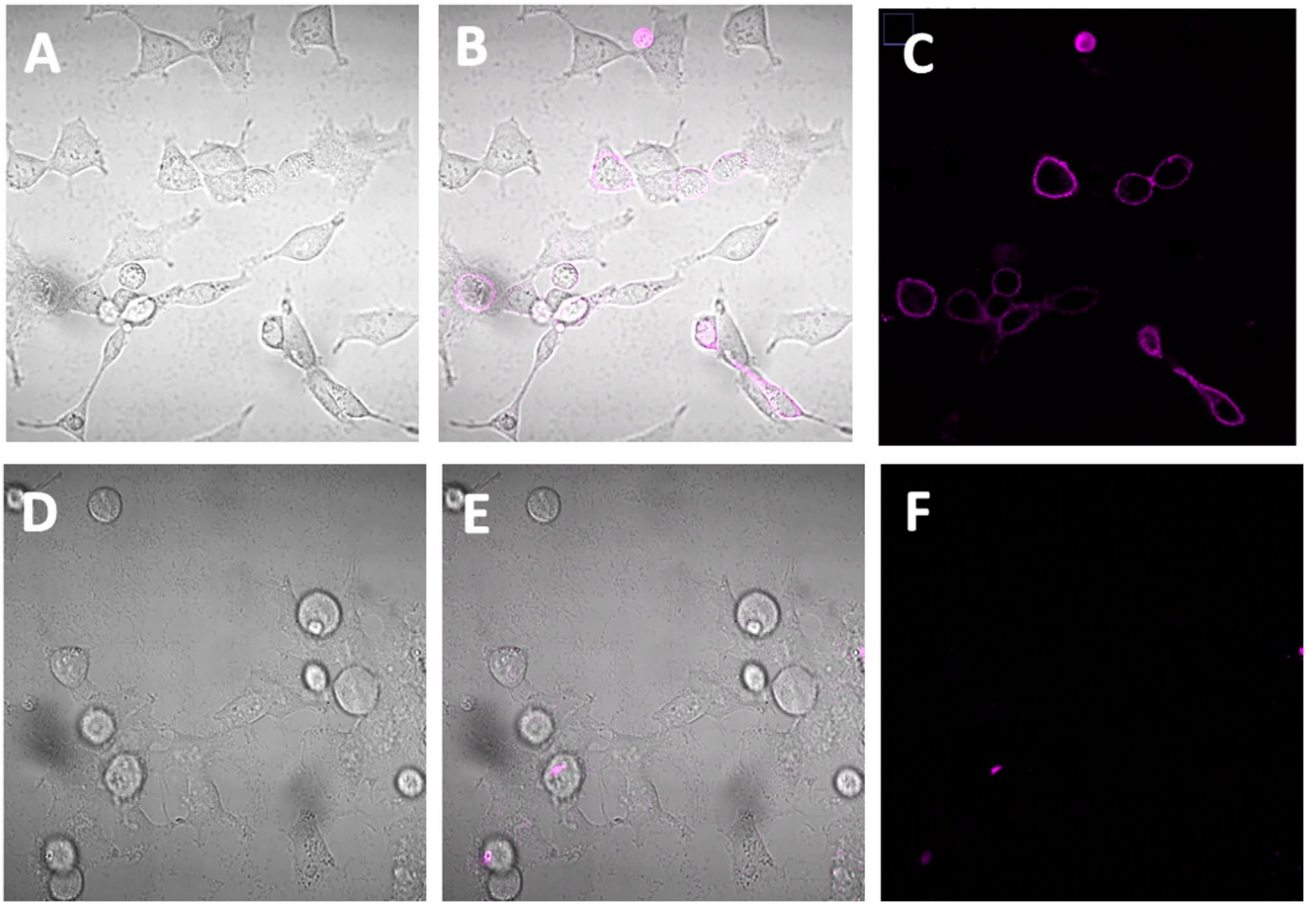

Fig. 7 Confocal microscopy images of HEK293 cells transfected with $hA_{2A}AR$ (transient). (A) and (D) are bright field images, (B) and (E) are bright field images with fluorescent overlay, and (C) and (F) are fluorescent images. The cells in images (A), (B), and (C) were treated with **12** (500 nM) for 1 h at 37 °C to measure the total binding of **12**. The cells in images (D), (E), and (F) were treated with both **12** (500 nM) and XAC (50 μM) to measure the non-specific binding of **12**

$A_{2A}AR$ binding by non-selective AR antagonist, XAC, and $A_{2A}AR$-selective agonist, CGS21680, was determined using FCM. The sigmoidal inhibition curves indicated K_i values of 53 and 783, respectively, compared to K_i values of 38.3 and 16.3 nM using an agonist radioligand [13]. Thus, the affinity determined for antagonist XAC was similar to previous values, but not the affinity of agonist CGS21680, using this antagonist fluorescent ligand. By comparison, the inhibition of the $hA_{2A}AR$ binding in whole cells using fluorescent antagonist **6** by agonists was complex, possibly due to multiple affinity states of this GPCR for agonists [10]. The cell images (Fig. 7B, C) show specific binding on the outer cell membrane, which disappeared when 50 μM XAC was present to block the fluorescent binding (Fig. 7E, F). Some cells showed no binding, which is reasonable considering that a transient transfection of the HEK293 cells was used.

Computational studies The hA_3AR interaction with antagonists was previously modeled using computational docking based on X-ray crystallographic structures of an antagonist-bound $hA_{2A}AR$ (PDB ID: 4EIY) [35, 36]. Here, a hypothetical binding mode was predicted for compound **19** at hA_3AR orthosteric binding site using molecular docking based on a structurally similar template (Fig. 8). The structure of hA_3AR was obtained through homology modeling, using as template an antagonist-bound hA_1AR structure in the inactive state (PDB ID: 5UEN [29]), as recently reported [28]. The model was previously optimized by induced fit docking of the known hA_3AR antagonist MRS1220 ($K_i \approx 0.7$ nM), which shares with compound **19** the 9-chloro-2-(2-furanyl)-[1,2,4]triazolo[1,5-c]quinazolin-5-amido scaffold [28]. The maximum common substructure between compound **19** and MRS1220 was used to constrain the docking search of compound **19**. The predicted pose of the ligand interacts with F168 (EL2) through a π-π stacking interaction, with N250 (TM6) through a bidentate H-bond engaging *N3* and the amido group at position 5. The carbonyl oxygen of the 5-amido group can be stabilized by a H-bond with Q167 on EL2, and further interactions of extracellular residues may involve the Sulfo-Cy7 group: in particular, in the predicted

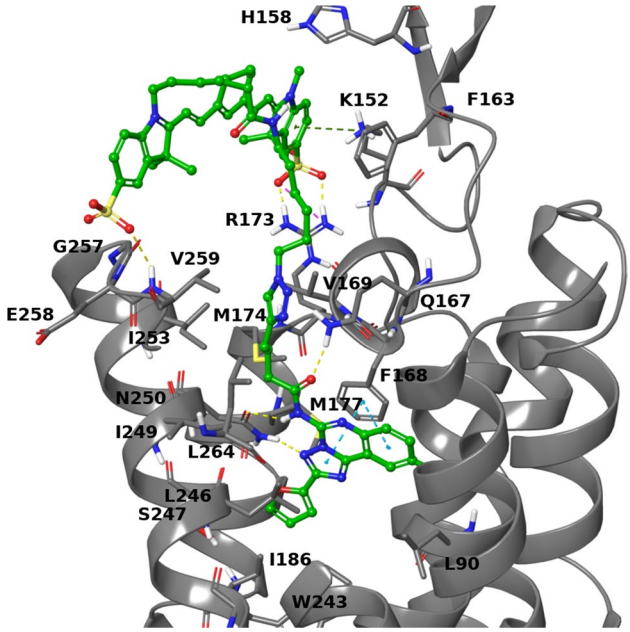

Fig. 8 Docking pose of compound **19** (C atoms in green) at the hA_3AR (gray) orthosteric binding site. Residues within 3 Å of the ligand are shown as sticks

poses, the two sulfonic groups are interacting through a H-bond with the amido group of V259 on EL3 and through an ionic H-bond with the side chain of R173 in EL2. Since the linker connecting the fluorophore to the triazoloquinazoline scaffold is flexible and its interactions are solvent exposed, we expect them just to be transient and not to contribute extensively to the ligand stabilization. The flexibility and lack of stable interactions of a fluorophore-conjugated moiety is pointed out in a recently determined X-ray structure of a stabilized $hA_{2A}AR$ bound to a BODIPY-conjugated pyrazolo[4,3-e]-1,2,4-triazolo[1,5-c] pyrimidine high affinity antagonist, which was the first X-ray structure of a GPCR bound to a fluorophore-conjugated ligand [37]. The chain linking the fluorophore to the *N7*-position of the pyrazolotriazolopyrimidine scaffold folds back upon the ELs of the receptor, pointing out of the orthosteric pocket, but the fluorophore could not be unambiguously solved because of the high flexibility of the linker. Instead, the triazolopyrimidine scaffold assumes the typical pattern of interactions at the $hA_{2A}AR$ involving the bidentate hydrogen bond with N253 (TM6) and π-π interaction with F168(EL2), resembling the predicted binding mode of the triazolopyrimidine substructure of compound **19** at hA_3AR binding site.

Discussion

Since the first instance of fluorescence observed for a chemical compound, i.e., quinine in 1845, much of the innovation of new specialized fluorophores has been driven by the proven utility of fluorescent compounds as biomolecular labels, cellular stains, and mechanistic probes [25, 38–40]. Part of the impetus to develop high affinity fluorescent ligands for ARs also arose from the cost and regulatory restrictions associated with the use of radioligands. Widespread availability of robust fluorescent AR ligands would make this research more economical and accessible to researchers worldwide.

Currently, rhodamine dyes are one of the most useful classes of fluorescent small molecules due to their brightness, the ease by which a large library of spectrally diverse dyes can be made through structural modification, and their characteristic chemical transformation from the non-fluorescent lactone form to the fluorescent zwitterionic form upon binding to their molecular target [25, 40]. Upon fluorophore binding, the lactone-zwitterion equilibrium is shifted toward the fluorescent zwitterion form, such that bound ligand fluoresces while non-bound ligand remains colorless [40]. This property of modified rhodamine dyes potentially eliminates the need for washing excess ligand when conducting cell imaging and binding studies [40]. One such rhodamine fluorophore is JF646, which can be easily coupled via the NHS ester to a wide variety of agonists and antagonists for live cell imaging and pharmacological characterization of different cellular receptors [40].

Fluorescent $A_{2A}AR$ antagonist **12**, which contains the JF646 fluorophore, was effective as a high-affinity flow cytometry probe for the $A_{2A}AR$ (K_d 222 ± 64 nM). The success of **12** in flow cytometric competitive binding assays with canonical antagonist XAC suggested that **12** is a suitable $A_{2A}AR$ fluorescent ligand for antagonist drug screening. Competitive binding of **12** with agonist CGS21680 did follow monophasic, sigmoidal inhibition. Thus, agonist screening using **12** appears to be more complex than antagonist screening. The potential of **12** as an $A_{2A}AR$ dye for fluorescent confocal microscopy was also confirmed, with **12** efficiently labeling the $hA_{2A}AR$ in a specific manner. The selective activation of JF646 fluorescent activity only upon binding of the ligand to its molecular target, allowed for wash free imaging of $hA_{2A}AR$ in live cells.

Fluorescent A_3AR antagonist **19** (K_d 11.8 ± 0.7 nM), containing the NIR Sulfo-Cy7, displayed high affinity and modest selectivity (11-fold vs. $A_{2A}AR$, roughly 50-fold vs. A_1AR and $A_{2B}AR$) and a good specific-to-nonspecific binding ratio. While **19** was demonstrated to be an effective flow cytometric probe for the A_3AR, the high excitation wavelength required to obtain a strong fluorescent emission signal presents a challenge since many flow cytometers are not equipped with far-red lasers. The greatest potential of **19** could be its application for in vivo imaging as a diagnostic NIR agent for imaging and/or therapy targeting the A_3AR [41, 42], although extensive pharmacokinetic characterization and additional control experiments would be required for in vivo studies. Near infrared light is particularly well

suited for in vivo imaging because of the low levels of biomolecular absorption and general cell autofluorescence in this wavelength range [43]. NIR fluorophore-tagged GPCR ligands have been used for live-cell imaging experiments, for example, the human orexin type 2 receptor [44]. A Cy5.5 fluorophore conjugated to a peripherally selective, high affinity agonist of long half-life was used to image the oxytocin receptor in living mice [45].

Conclusions

We have introduced novel fluorescent conjugates of known AR pharmacophore functionalized congeners in two chemical series, 8-aryl-1,3-dialkylxanthines and triazolo[1,5-c]quinazolin-5-yl)amine. Among the conjugates synthesized and characterized are a JF probe **12**, which binds and can be imaged at the A_{2A}AR in whole cells, and an A_3AR NIR antagonist probe **19**, containing a Sulfo-Cy7 NIR dye, of even higher affinity, which can be used as a screening tool in flow cytometry for drug discovery. We also predicted a bitopic interaction mode of **19** with an A_3AR homology model.

Supplementary Information The online version contains supplementary material available at https://doi.org/10.1007/s11302-022-09873-3.

Acknowledgements We thank Dr. Martin J. Schnermann, NCI, Frederick, for a generous supply of FNIR-Tag-NHS ester. We thank Tocris for the gift of JF dyes. We thank the NIDDK Advanced Light Microscopy & Image Analysis Core (ALMIAC) for the use of its resources and its director Jeff Reece for helpful discussions.

Funding National Institute of Diabetes and Digestive and Kidney Diseases, Intramural Research Program (grant no. ZIADK031117).

Data availability The original data from this study will be made available upon reasonable request.

Declarations

Conflict of interest Kiran S. Toti declares that he has no conflict of interest. Ryan G. Campbell declares that she has no conflict of interest. Hobin Lee declares that she has no conflict of interest. Veronica Salmaso declares that she has no conflict of interest. R. Rama Suresh declares that he has no conflict of interest. Zhan-Guo Gao declares that he has no conflict of interest. Kenneth A. Jacobson declares that he has no conflict of interest.

Ethical approval Not applicable; no animal studies are included.

Consent to participate Not applicable; no patient studies are included.

References

1. Baker JG, Middleton R, Adams L, May LT, Briddon SJ, Kellam B, Hill SJ (2010) Influence of fluorophore and linker composition on the pharmacology of fluorescent adenosine A_1 receptor ligands. Br J Pharmacol 159:772–786
2. Ciruela F, Fernández-Dueñas V, Jacobson KA (2015) Lighting up G protein-coupled purinergic receptors with engineered fluorescent ligands. Neuropharmacology 98:58–67
3. Comeo E, Kindon ND, Soave M, Stoddart LA, Kilpatrick LE, Scammells PJ, Hill SJ, Kellam B (2020) Subtype-selective fluorescent ligands as pharmacological research tools for the human adenosine A_{2A} receptor. J Med Chem 63:2656–2672
4. McCabe RT, Skolnick P, Jacobson KA (1992) 2-[2-[4-[2-[2-[1,3-Dihydro-1,1-bis (4-hydroxyphenyl)-3-oxo-5-isobenzofuranthioureidyl]ethylaminocarbonyl]ethyl]phenyl]-ethylamino]-5′-N-ethylcarboxamidoadenosine (FITC-APEC): a fluorescent ligand for A_2-adenosine receptors. J Fluoresc 2:217–223
5. Fernández-Dueñas V, Gómez-Soler M, Jacobson KA, Kumar TS, Fuxe K, Borroto-Escuela DO, Ciruela F (2012) Molecular determinants of the adenosine A_{2A}R-dopamine D_2 receptor-receptor allosterism: role of the intracellular loop 3 of the dopamine D_2 receptor. J Neurochem 123:373–384
6. May LT, Bridge LJ, Stoddart LA, Briddon SJ, Hill SJ (2011) Allosteric interactions across native adenosine-A_3 receptor homodimers: quantification using single-cell ligand-binding kinetics. FASEB J 25:3465–3476
7. Briddon SJ, Middleton RJ, Cordeaux Y, Flavin FM, Weinstein JA, George MW, Kellam B, Hill SJ (2004) Quantitative analysis of the formation and diffusion of A_1-adenosine receptor-antagonist complexes in single living cells. Proc Natl Acad Sci USA 101:4673–4678
8. Kozma E, Kumar TS, Federico S, Phan K, Balasubramanian R, Gao ZG, Paoletta S, Moro S, Spalluto G, Jacobson KA (2012) Novel fluorescent antagonist as a molecular probe in A_3 adenosine receptor binding assays using flow cytometry. Biochem Pharmacol 83:1552–1561
9. Vernall AJ, Stoddart LA, Briddon SJ, Ng HW, Laughton CA, Doughty SW, Hill SJ, Kellam B (2013) Conversion of a non-selective adenosine receptor antagonist into A_3-selective high affinity fluorescent probes using peptide-based linkers. Org Biomol Chem 11:5673–5682
10. Duroux R, Ciancetta A, Mannes P, Yu J, Boyapati S, Gizewski E, Yous S, Ciruela F, Auchampach JA, Gao ZG, Jacobson KA (2017) Bitopic fluorescent antagonists of the A_{2A} adenosine receptor based on pyrazolo[4,3-e][1,2,4]triazolo[1,5-c]pyrimidin-5-amine functionalized congeners. Med Chem Commun 8:1659–1667
11. Bouzo-Lorenzo M, Stoddart LA, Xia L, IJzerman AP, Heitman LH, Briddon SJ, Hill SJ (2019) A live cell NanoBRET binding assay allows the study of ligand-binding kinetics to the adenosine A_3 receptor. Purinergic Signal 15:139–153
12. Federico S, Margiotta E, Moro S, Kozma E, Gao ZG, Jacobson KA, Spalluto G (2020) Conjugable A_3 adenosine receptor antagonists for the development of functionalized ligands and their use in fluorescent probes. Eur J Med Chem 186:11188
13. Gao ZG, Toti KS, Campbell R, Suresh RR, Yang H, Jacobson KA (2020) Allosteric antagonism of the A_{2A} adenosine receptor by a series of bitopic ligands. Cells 9:1200
14. Köse M, Gollos S, Karcz T, Fiene A, Heisig F, Behrenswerth A, Kieć-Kononowicz K, Namasivayam V, Müller CE (2018) Fluorescent-labeled selective adenosine A_{2B} receptor antagonist enables competition binding assay by flow cytometry. J Med Chem 61:4301–4316
15. Stoddart LA, Kindon ND, Otun O, Harwood CR, Patera F, Veprintsev DB, Woolard J, Briddon SJ, Franks HA, Hill SJ, Kellam B (2020) Ligand-directed covalent labelling of a GPCR with a fluorescent tag in live cells. Commun Biol 3:722

16. Jacobson KA, Tosh DK, Jain S, Gao ZG (2019) Historical and current adenosine receptor agonists in preclinical and clinical development. Frontiers Cell Neurosci 13:124
17. Boison D, Rho JM (2020) Epigenetics and epilepsy prevention: The therapeutic potential of adenosine and metabolic therapies. Neuropharmacology 167:107741
18. Martí Navia A, Dal Ben D, Lambertucci C, Spinaci A, Volpini R, Marques-Morgado I, Coelho JE, Lopes LV, Marucci G, Buccioni M (2020) Adenosine receptors as neuroinflammation modulators: role of A_1 agonists and A_{2A} antagonists. Cells 9:1739
19. Sacramento JF, Martins FO, Rodrigues T, Matafome P, Ribeiro MJ, Olea E, Conde SV (2020) A_2 adenosine receptors mediate whole-body insulin sensitivity in a prediabetes animal model: primary effects on skeletal muscle. Frontiers Endocrinol 11:262
20. Yu F, Zhu C, Xie Q, Wang Y (2020) Adenosine A_{2A} receptor antagonists for cancer immunotherapy. J Med Chem 63:12196–12212
21. de Oliveira M, Mathias LS, de Sibio MT, Noronha-Matos JB, Costa MA, Nogueira CR, Correia-de-Sá P (2020) Pitfalls and challenges of the purinergic signaling cascade in obesity. Biochem Pharmacol 182:114214
22. Jacobson KA, Ukena D, Kirk KL, Daly JW (1986) [^{3}H]Xanthine amine congener of 1,3-dipropyl-8-phenylxanthine: an antagonist radioligand for adenosine receptors. Proc Natl Acad Sci USA 83:4089–4093
23. Kim YC, de Zwart M, Chang L, Moro S, von Frijtag Drabbe Künzel JK, Melman N, IJzerman AP, Jacobson KA (1998) Derivatives of the triazoloquinazoline adenosine antagonist (CGS15943) having high potency at the human A_{2B} and A_3 receptor subtypes. J Med Chem 41:2835–2841
24. Jacobson KA, IJzerman AP, Müller CE (2021) Medicinal chemistry of P2 and adenosine receptors: common scaffolds adapted for multiple targets, Biochem. Pharmacol 187:114311
25. Grimm JB, Muthusamy AK, Liang Y, Brown TA, Lemon WC, Patel R, Lu R, Macklin JJ, Keller PJ, Ji N, Lavis LD (2017) A general method to fine-tune fluorophores for live-cell and in vivo imaging. Nature Meth 14:987–994
26. Luciano MP, Crooke SN, Nourian S, Dingle I, Nani RR, Kline G, Patel NL, Robinson CM, Difilippantonio S, Kalen JD, Finn MG, Schnermann MJ (2019) A nonaggregating heptamethine cyanine for building brighter labeled biomolecules. ACS Chem Biol 14:934–940
27. Inverarity IA, Viguier RFH, Cohen P, Hulme AN (2007) Biotinylated anisomycin: a comparison of classical and "click" chemistry approaches. Bioconjugate Chem 18:1593–1603
28. Suresh RR, Gao ZG, Salmaso V, Chen E, Campbell RG, Poe RB, Liston TE, Jacobson KA (2022) Selective A_3 adenosine receptor antagonist radioligand for human and rodent species. ACS Med Chem Lett 13(4):623–631
29. Glukhova A, Thal DM, Nguyen AT, Vecchio EA, Jörg M, Scammells PJ, May LT, Sexton PM, Christopoulos A (2017) Structure of the adenosine A_1 receptor reveals the basis for subtype selectivity. Cell 168:867–877
30. Sastry GM, Adzhigirey M, Day T, Annabhimoju R, Sherman W (2013) Protein and ligand preparation: parameters, protocols, and influence on virtual screening enrichments. J Comput Aided Mol Des 27:221–234. https://doi.org/10.1007/s10822-013-9644-8
31. Schrödinger Release 2021–2: Maestro; Schrödinger, LLC: New York, NY, 2021.
32. Friesner RA, Banks JL, Murphy RB, Halgren TA, Klicic JJ, Mainz DT, Repasky MP, Knoll EH, Shelley M, Perry JK, Shaw DE, Francis P, Shenkin PS (2004) Glide: a new approach for rapid, accurate docking and scoring. 1. Method and assessment of docking accuracy. J Med Chem 47:1739–1749. https://doi.org/10.1021/jm0306430
33. Halgren TA, Murphy RB, Friesner RA, Beard HS, Frye LL, Pollard WT, Banks JL (2004) Glide: a new approach for rapid, accurate docking and scoring. 2. Enrichment factors in database screening. J Med Chem 47:1750–1759 https://doi.org/10.1021/jm030644s.
34. Friesner RA, Murphy RB, Repasky MP, Frye LL, Greenwood JR, Halgren TA, Sanschagrin PC, Mainz DT (2006) Extra precision glide: docking and scoring incorporating a model of hydrophobic enclosure for protein-ligand complexes. J Med Chem 49:6177–6196 https://doi.org/10.1021/jm051256ox
35. Yu J, Mannes P, Jung YH, Ciancetta A, Bitant A, Lieberman DI, Khaznadar S, Auchampach JA, Gao ZG, Jacobson KA (2018) Structure activity relationship of 2-arylalkynyl-adenine derivatives as human A_3 adenosine receptor antagonists. Med Chem Commun 9:1920–1932
36. Tosh DK, Salmaso V, Rao H, Bitant A, Fisher CL, Lieberman DI, Vorbrüggen H, Reitman ML, Gavrilova O, Gao ZG, Auchampach JA, Jacobson KA (2020) Truncated (N)-methanocarba nucleosides as partial agonists at mouse and human A_3 adenosine receptors: Affinity enhancement by N^6-(2-phenylethyl) substitution. J Med Chem 63:4334–4348
37. Claff T, Klapschinski TA, Tiruttani Subhramanyam UK, Vaaßen VJ, Schlegel JG, Vielmuth C, Voß JH, Labahn J, Müller CE (2022) Single stabilizing point mutation enables high-resolution co-crystal structures of the adenosine A_{2A} receptor with preladenant conjugates. Angew Chem Int Ed e202115545
38. Herschel JFW (1845) On a case of superficial colour presented by a homogeneous liquid internally colourless. Phil Trans R Soc 135:143–145
39. Lu L, Wu Zy, Li X, Han F (2019) State-of-the-art: functional fluorescent probes for bioimaging and pharmacological research. Acta Pharmacol Sin 40:717–723.
40. Zheng Q, Ayala AX, Chung I, Weigel AV, Ranjan A, Falco N, Grimm JB, Tkachuk AN, Wu C, Lippincott-Schwartz J, Singer RH, Lavis LD (2019) Rational design of fluorogenic and spontaneously blinking labels for super-resolution imaging. ACS Central Sci 5:1602–1613
41. Yan C, Zhang Y, Guo Z (2021) Recent progress on molecularly near-infrared fluorescent probes for chemotherapy and phototherapy. Coordination Chem Rev 427:213556
42. Baues M, Klinkhammer BM, Ehling J, Gremse F, van Zandvoort MAMJ, Reutelingsperger CPM, Daniel C, Amann K, Bábíčková J, Kiessling F, Floege J, Lammers T, Boor P (2020) A collagen-binding protein enables molecular imaging of kidney fibrosis in vivo. Kidney Internat 97:609–614
43. Weissleder RA (2001) Clearer vision for in vivo imaging. Nature Biotechnol 19:316–317
44. Lesiak L, Zhou X, Fang Y, Zhao J, Beck JR, Stains CI (2020) Imaging GPCR internalization using near-infrared Nebraska red-based reagents. Org Biomolec Chem 18:2459–2467
45. Esteoulle L, Daubeuf F, Collot M, Riché S, Durroux T, Brasse D, Marchand P, Karpenko JA, Klymchenko SA, Bonnet D (2020) A near-infrared fluorogenic dimer enables background-free imaging of endogenous GPCRs in living mice. Chemical Sci 11:6824–6829
46. Kecskés A, Tosh DK, Wei Q, Gao ZG, Jacobson KA (2011) GPCR ligand dendrimer (GLiDe) conjugates: Adenosine receptor interactions of a series of multivalent xanthine antagonists. Bioconjugate Chem 22:1115–1127